Available online at www.sciencedirect.com
SCIENCE DIRECT®
Sensors and Actuators A 112 (2004) 175–183
SENSORS AND ACTUATORS A PHYSICAL
www.elsevier.com/locate/sna

LIGA fabricated 19-element threshold accelerometer array

Shamus McNamara [a,b,*], Yogesh B. Gianchandani [a,b]

[a] *Department of Electrical and Computer Engineering, University of Wisconsin, Madison, WI, USA*
[b] *1301 Beal Avenue, Department of Electrical Engineering and Computer Science, University of Michigan, Ann Arbor, MI 48109, USA*

Received 22 July 2002; accepted 27 October 2003

Abstract

This paper reports the design, fabrication, packaging, and testing of a relay-type threshold accelerometer array. The array includes 15 different sense elements ranging from 10 to 150 g in 10 g increments, and triply redundant 20 and 100 g sense elements for a total of 19 elements. The devices were fabricated using a modified sacrificial LIGA technique that creates a 100–300 μm thick nickel structure with gold plated contacts. The threshold accelerometer array was evaluated by measuring its response to an applied acceleration (using a centrifuge) and by using two built-in testing methods: a pull-in voltage test, and a transit time test. Unlike the pull-in voltage test, the transit time test is sensitive to variations in the proof mass and spring constant. The average results from the centrifuge test, pull-in voltage test, and transit time test are all within approximately 20% of the expected values that are analytically calculated. In addition to the relay-type threshold sensing, the devices permit non-discretized readout of the acceleration using an alternative sense mode, in which the capacitance between the test electrode and proof mass was measured. This measurement shows a sensitivity of 670 aF/g for a 50 g threshold accelerometer, which is also within 20% of theoretical estimates.

Keywords: Accelerometer; Spring constant; Bi-directional sensing

1. Introduction

Research into micromachined accelerometers has been ongoing both commercially and academically for the last several decades [1]. Threshold accelerometers are typically designed with a proof mass and a restoring spring. At a pre-selected threshold, the force on the proof mass will be sufficient to overcome the force due to the restoring spring and the proof mass will come into contact with another electrode, making an electrical contact. Thus, the operation of a threshold accelerometer is related to that of a relay. The discrete output, coupled with the simple switch-like behavior, allows for a very simple interface circuit and very low power consumption. This permits long-term operation from a small battery. Since a threshold accelerometer triggers at a single threshold, an array is necessary to provide a wide acceleration range [2–6].

Most threshold accelerometers reported in the past have been designed to detect out-of-plane accelerations. For a number of applications this is less desirable than sensing in the substrate-plane, which can simplify mounting and alignment. It also simplifies bi-directional sensing (i.e. along the positive and negative direction of the sense axis) because electrodes can be in the same plane as the proof mass and only one structural layer is required. There is only one report of a substrate-plane sensing device in the past, but it targets very high g-forces [2].

Sensitivity (defined in this context as the lowest acceleration threshold) and reliability have been the largest obstacles to the fabrication of the threshold accelerometer. The highest sensitivity working threshold accelerometer reported in the past required a minimum acceleration of 400 g to trigger [3]. However, many applications require sensitivities well below 100 g. For example airbag systems on cars trigger at 50 g. As the sensitivity is increased, it becomes less robust because the restoring spring has to become weaker. Thus, most reported working threshold accelerometers have low sensitivity and target 1000's of *g*'s [2–5].

Another reliability concern is the opening and closing of the electrical contact [4]. According to previous reports the contacts often have not closed because of warping of the beams, or because a multiple contact scheme is used and only one contact closes. Furthermore, the contacts often do not open because of inadequate restoring force in the deflected beam to overcome the adhesive forces due to stiction or micro-welding at the contact.

* Corresponding author.

0924-4247/$ – see front matter © 2003 Elsevier B.V. All rights reserved.
doi:10.1016/j.sna.2003.10.064

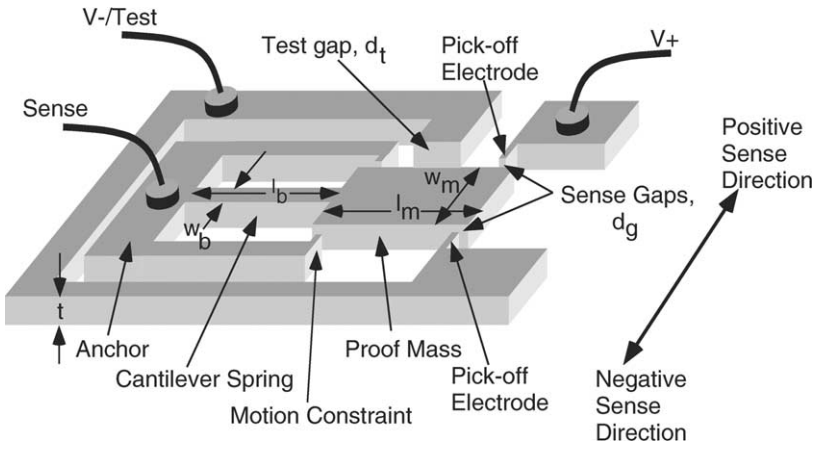

Fig. 1. Schematic illustrating the major components of the threshold accelerometer.

This paper presents a 19-element threshold accelerometer array that senses acceleration thresholds over the range of 10–150 g in 10 g increments [7,8].[1] Of the 19 elements, 15 are unique designs out of which two designs are triply redundant for better fault tolerance. Each element is a substrate-sensing device that detects accelerations along a single sense axis. The 10 g threshold provides the highest threshold sensitivity reported in a contact switch type device to date. The reliability concern has also been addressed by a number of features of the structure and of the fabrication method used. Furthermore, the threshold accelerometer has provisions for two types of built-in test, the standard pull-in voltage test and a new transit-time test. This new transit-time test is a more thorough test than the pull-in voltage test. The threshold accelerometer array has been fabricated using a variant of the sacrificial LIGA process [9] to create gold plated nickel structures that are hundreds of micrometers thick. The device structure and theory of operation are explained in Section 2. The fabrication procedure is given in Section 3. Experimental results are given in Section 4, and the conclusions are given in Section 5.

2. Structure and operation

The schematic of the threshold accelerometer shown in Fig. 1 illustrates the following important components: proof mass, cantilever spring, anchor, $V+$ pick-off electrode, $V-$ pick-off electrode, test electrode, and two bumpers. A sense gap (d_g) exists between the proof mass and the two pick-off electrodes and a test gap (d_t) is located between the proof mass and test electrode. The $V+$ pick-off electrode is used to detect accelerations in the positive direction, and the $V-$ pick-off electrode is used to detect accelerations in the negative direction. To save on the pin count of a packaged device, the test electrode and $V-$ pick-off electrodes utilize the same lead. Alignment errors are eliminated because all the structures are defined in a single mask layer. The proof mass and cantilever spring are aligned perfectly and the proof mass is exactly centered between the pick-off electrodes. The proof mass is designed to be narrow to minimize the cross-axis sensitivity (as explained below). The cantilever spring is very thick (100–300 μm) to provide low cross-axis sensitivity in the out-of-plane direction, to be reliable and robust, and to provide a strong restoring force to open the contact when the applied acceleration drops below the threshold value. The pick-off electrodes and bumpers constrain the proof mass so that the cantilever spring cannot be bent beyond its elastic limit. Furthermore, the pick-off electrodes and bumpers prevent the proof mass from touching the test electrode during built-in testing or during handling. The test electrode is positioned at the center of the proof mass, and the test electrode is segmented in order to reduce the magnitude of the squeeze film damping due to the small gap between the test electrode and the proof mass.

The threshold accelerometer triggers when the force on the proof mass due to an applied acceleration is sufficient to deflect the restoring spring across the sense gap [1]:

$$a_t = \frac{E w_b^3 d_g}{\rho\, w_m l_m l_b}\left[\frac{1}{4l_b^2 + 9l_b l_m + 6l_m^2}\right] \quad (1)$$

where the physical dimensions l_m, l_b, w_m, w_b, and d_g are labeled in Fig. 1, a_t is the acceleration threshold, E is the Young's modulus of the cantilever spring, and ρ is the density of the proof mass. An advantage of this structure is that the acceleration threshold is independent of the thickness, allowing greater fabrication latitude. This is because the proof mass and cantilever spring are the same thickness.

The threshold accelerometer array was designed by holding all the dimensions constant except for the cantilever spring length in order to match any source of variability across the whole array. It was necessary to use two sizes of proof masses to keep the cantilever spring to a length of less than 1 mm. A proof mass of 60 μm wide (w_m) and 600 μm long (l_m) was used for the sense elements from 50 to 150 g,

[1] Portions of this paper have appeared in conference abstract form in [7].

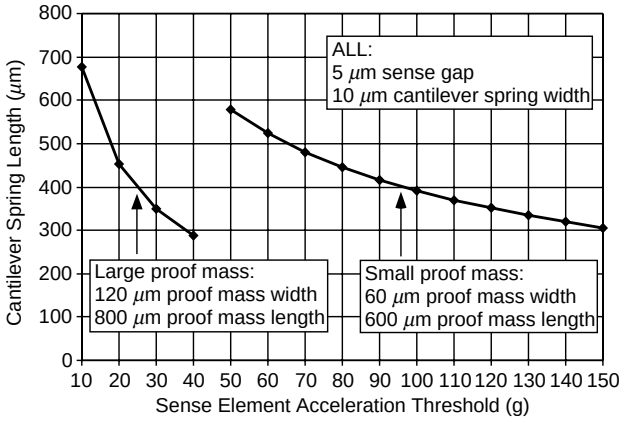

Fig. 2. Cantilever spring length for all 15 unique sense elements.

whereas a larger mass of 120 μm wide (w_m) and 800 μm long (l_m) was used for the sense elements from 10 to 40 g. A relatively small proof mass width was selected to reduce cross-axis sensitivity. The sense gap was 5 μm and the cantilever spring was 10 μm wide because that is the minimum size that the LIGA fabrication technique will permit with a high yield. The lengths of all the cantilever springs may be found in Fig. 2. The structural thickness (t) was 100–300 μm. This thickness provides for minimal out-of-plane deflection due to internal and external forces.

2.1. Built-in tests

The built-in test method typically used for devices such as the threshold accelerometer is the pull-in voltage test. When a voltage is applied to the test electrode with the proof mass grounded, an electrostatic force is generated that pulls the proof mass in toward the test electrode. Fig. 3 shows the cantilever spring restoring force and the electrostatic force for

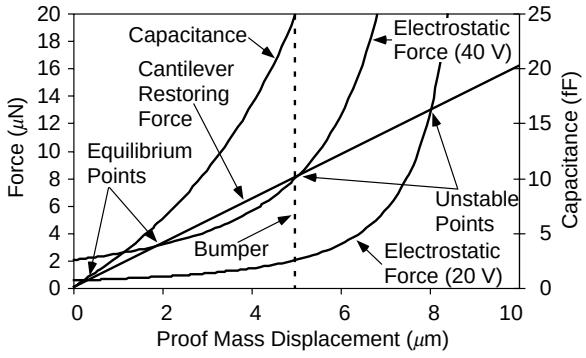

Fig. 3. The curves on the graph show the cantilever restoring force and the electrostatic force (at 20 and 40 V applied to the test electrode) as a function of the proof mass displacement. The locations where the net force is zero (the cantilever restoring force equals the electrostatic force) may be either stable or unstable. The capacitance (axis on right side) is also shown as a function of proof mass displacement. Physically, the proof mass can only displacement 5 μm because a bumper is located at one end and a pick-off electrode at the other end of the proof mass.

two voltages as a function of distance. For a given voltage, there are two locations where the net force is zero (spring restoring force equals the electrostatic force). At 20 V, the two null-force locations consist of a stable displacement of 0.3 μm and an unstable displacement at 8 μm. The 8 μm location is unstable because the force at any position on the graph to the left of it will result in movement toward the stable point and any position to the right will result in movement toward the test electrode. Of course, the bumpers and pick-off electrodes limit the range of motion so the proof mass can never deflect to the 8 μm location. Further increases in the applied voltage will increase the electrostatic force, moving the stable point to the right and the unstable point to the left (see the intersections between the spring restoring force and the 40 V electrostatic force). At some critical voltage, called the pull-in voltage, there are no stable solutions and the proof mass will be pulled in toward the test electrode. This voltage is uniquely determined by the device dimensions and material properties, and thus forms the basis behind the pull-in voltage built-in test. To implement the test an applied voltage is slowly ramped until the proof mass contacts the pick-off electrode. The pull-in voltage can be approximated as [10]

$$V_{\text{pull-in}} = \sqrt{\frac{2Ew_b^3 d_t^3}{27\varepsilon_0 l_t l_b (4l_b^2 + 6l_b l_m + 3l_m^2)}} \quad (2)$$

where ε_0 is the dielectric constant of the medium between the proof mass and the test electrode and l_t is the length of the test electrode. Although this is an easy test to perform, it is limited in its ability to measure variations in the proof mass. The pull-in voltage test is independent of the proof mass width (w_m) and density (ρ), and has only a small dependence on its length (l_m). This means that process variations in the dimensions of the proof mass or in the density of the deposited material that may significantly affect the acceleration threshold may not be detected using the pull-in voltage test. It also cannot measure any parameters that only affect the dynamic response, such as the damping coefficient.

A transit-time test has been devised to overcome the limitations of the pull-in voltage test. A prescribed voltage that is greater than the pull-in voltage is applied as a step function to the test electrode, causing the proof mass to be deflected into the pick-off electrode. The time between the application of the test voltage and the first contact at the pick-off electrode is measured. This time is the transit time, and it depends on the spring constant, the mass of the proof mass (length, width, and density), and the damping coefficient. The transit time test is a more complete test than the pull-in voltage test because it provides a measure of not only the spring constant but also the proof mass. The theoretical transit time is found by numerically integrating the following equation:

$$M\frac{d^2y}{dt^2} = F_{\text{test}} - b\frac{dy}{dt} - k_{\text{spring}}y \quad (3)$$

where M is the total mass of the proof mass, y is the deflection of the tip of the proof mass, t is time, F_{test} is the applied electrostatic force, b is the damping coefficient, and k_{spring} is the spring constant of the cantilever spring. F_{test} and k_{spring} may be found from the following two equations [10]:

$$F_{\text{test}} = -\frac{\varepsilon_0 l_t t V^2}{2(d_t - y)^2} \tag{4}$$

$$k_{\text{spring}} = \frac{w_b^3 E t}{l_b} \frac{1}{4l_b^2 + 6l_b l_m + 3l_m^2} \tag{5}$$

where t is the structure thickness and V is the voltage applied between the test electrode and proof mass. Eq. (4) assumes that the proof mass moves approximately parallel to the test electrode. Analytical procedures for calculating the damping coefficient, b, have been reported elsewhere for viscous-film damping [11] and squeeze-film damping [12]. The two types of damping are then summed to get the total damping coefficient. Since the damping coefficient depends greatly on the geometry, analytical expressions for damping are often not very accurate. If the device dimensions and Young's modulus are known, and the density of the material is known, then a measured damping coefficient may be obtained by comparing the measured transit-time test results to theoretical transit-time test results for a variety of damping coefficients.

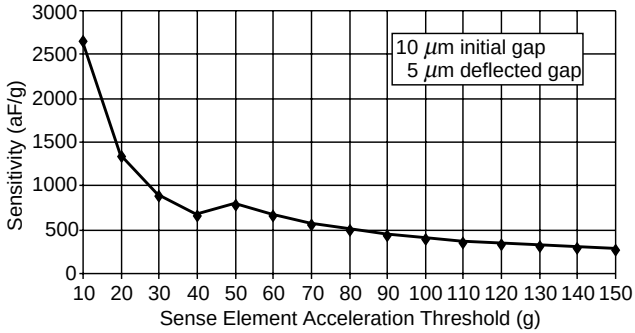

Fig. 4. Calculated sensitivity for the capacitive sense mode.

An acceleration larger than the threshold acceleration can be applied without triggering the threshold accelerometer, provided that the applied acceleration is sufficiently short. Eq. (3), which is used to solve for the transit time test, can also be solved to determine whether an acceleration applied for a very short time will cause the threshold accelerometer to be triggered. This is performed by inserting the applied

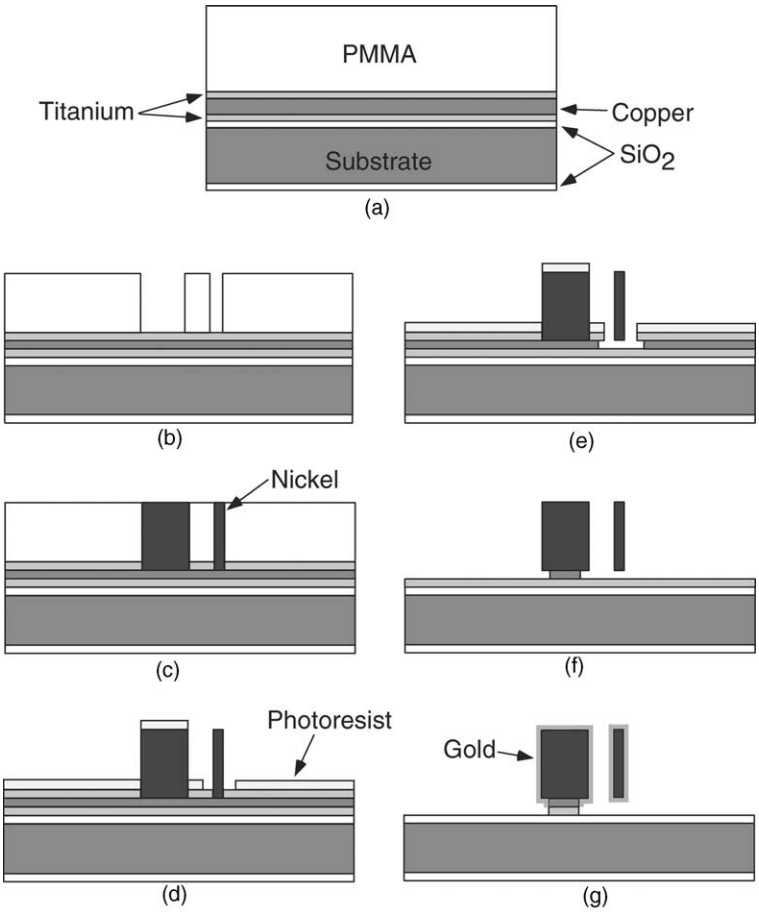

Fig. 5. Outline of the processing steps used to fabricate the threshold accelerometer.

force profile of interest in place of the applied test force F_{test}. For example, the 10 g threshold accelerometer will not be triggered by an acceleration of 20 g that only lasts 0.1 ms.

2.2. Capacitive sense mode

Although the sense structure was designed for discrete measurements in an array, they can also provide an analog output. This output is provided by the capacitance between the test electrode and the proof mass. As the proof mass deflects toward the test electrode, the capacitance between the electrodes increases (Fig. 3). The measurement range of the capacitive sense mode accelerometer is from zero to a maximum equal to the threshold acceleration, which occurs when the tip of the proof mass contacts the pick-off electrode at this acceleration. Assuming that the proof mass moves parallel to the test electrode, the total change in capacitance is given by

$$\Delta C = \varepsilon_0 l_t t_m \left(\frac{1}{d_g} - \frac{1}{d_t} \right) \quad (6)$$

The sensitivity of the device is defined as

$$S = \frac{\Delta C}{a_t} \quad (7)$$

where a_t is given in Eq. (1). Fig. 4 shows the expected sensitivity for all 15 different sense elements. The maximum sensitivity is 2.6 fF/g using a 10 g threshold accelerometer.

3. Fabrication

The threshold accelerometer array was fabricated using a two mask modified sacrificial LIGA process. The first mask simultaneously defines every structure, and the second mask helps during etch of the sacrificial layer. The structure is made out of electroplated nickel and coated with gold for a good electrical contact.

An outline of the fabrication process is shown in Fig. 5. The starting material is an insulating substrate, such as silicon with a thermally grown oxide or a glass substrate. The metal structures are formed using a typical LIGA process as follows [9]. A 200 Å layer of titanium, a 4.5 μm thick sacrificial layer of copper, and a 200 Å layer of titanium are sputtered on top of the substrate. A sheet of PMMA is then solvent bonded on top of the substrate and milled to the desired thickness (100–300 μm) using a fly-cutter (Fig. 5a). The sample is exposed to x-rays from a synchrotron source through an X-ray mask and developed (Fig. 5b). The exposed titanium is etched in an RIE reactor and nickel is electroplated into the PMMA mold (Fig. 5c). Finally, the PMMA is dissolved, leaving nickel structures attached to the substrate.

The selective release of the movable nickel structures is aided with the use of a second masking step. Photoresist is spun on the wafer, exposed on a UV mask aligner, and developed. The mask contains an opening for the proof mass (Fig. 5d). The exposed titanium is etched in dilute HF and the sacrificial copper layer is time etched to free the proof mass (Fig. 5e). The photoresist and titanium are then stripped from the sample and the copper is again time etched to remove the copper under the cantilever springs (Fig. 5f). The sample is selectively electroplated with gold and the remaining titanium is removed to electrically isolate all the components (Fig. 5g).

In order to create good electrical contacts, gold is electroplated over the nickel and copper structures. The titanium layer is left on the substrate during this step to electrically connect all the components to be electroplated. Because the different components must be electrically isolated in final form, the titanium must not be coated with gold so that it may be removed. This is accomplished by performing the electroplating at a low electropotential. The gold is selectively electroplated on the nickel and copper, but not on the titanium. This procedure works to apply thin layers of gold on the nickel and copper. The plating time (and hence thickness) must be monitored because, if the titanium layer gets coated with a layer of gold, the plating rate over the titanium will be the same as that over the nickel and copper, and the procedure will fail.

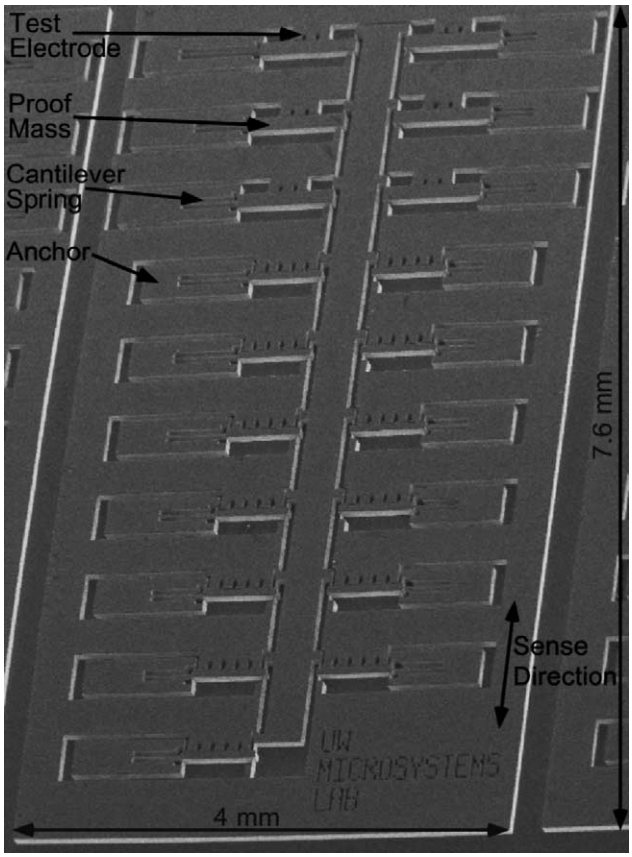

Fig. 6. SEM of the threshold accelerometer array showing all 19 sense elements (15 different elements plus two redundant 20 g elements and two redundant 100 g elements).

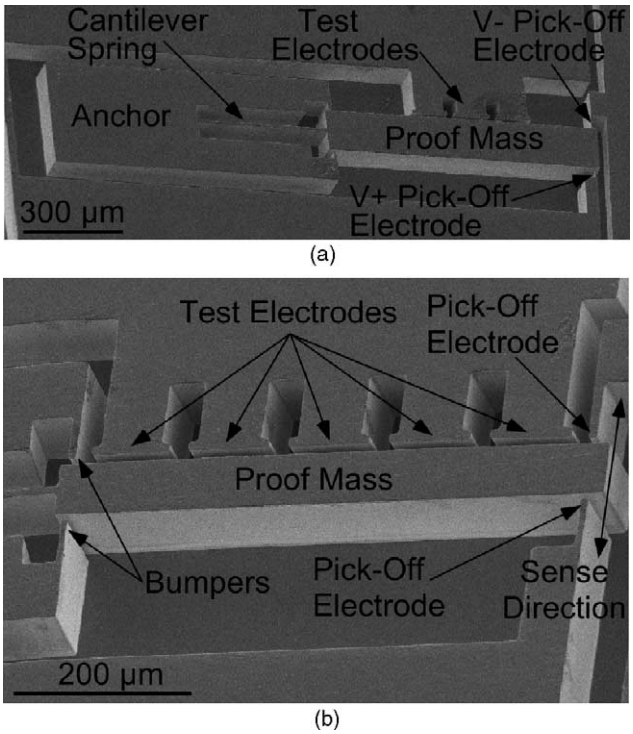

Fig. 7. Close-up SEMs of (a) large proof mass and (b) small proof mass threshold accelerometer.

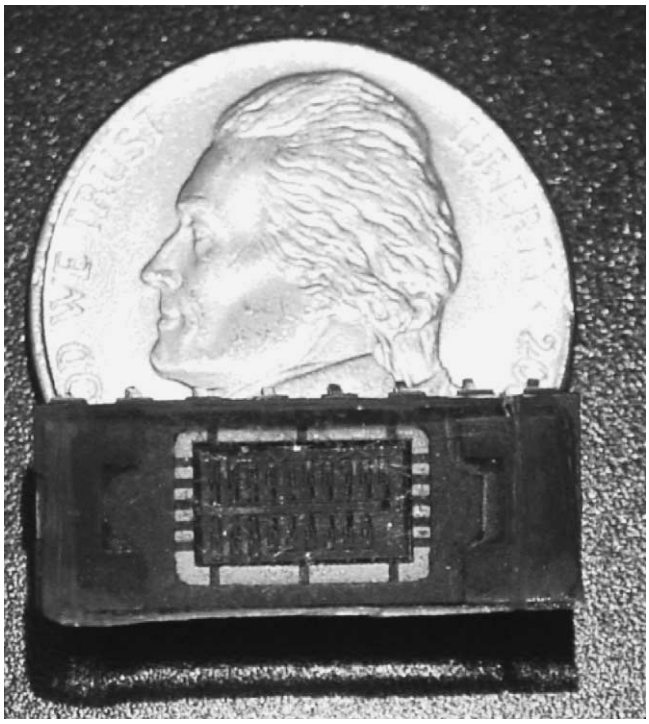

Fig. 8. Packaged threshold accelerometer with a transparent plastic lid compared to a US 5 cent piece.

Fig. 6 shows an SEM of the entire die before the last layer of titanium is removed. Fig. 7 shows close-up SEMs of two sense elements. Fig. 7a shows a sense element with a large proof mass and Fig. 7b shows a sense element with a small proof mass. There are several significant features that may be seen in Fig. 7. First, the test electrodes are segmented in order to increase the yield (by reducing the lengths of narrow segments of the PMMA mold) and reduce the effects of squeeze-film damping. The test electrode area of the small proof mass is much larger than that for the large proof mass. There are bumpers at the left side of the figure and pick-off electrodes at the right side of the figure. The separation between the proof mass and the test electrodes is greater than that between the proof mass and pick-off electrodes and greater than that between the proof mass and the bumpers. This prevents the proof mass from ever touching the test electrode. Fig. 8 shows a packaged device. Wirebonds are made between the package lead-frame and the anchors. In Fig. 8, a plastic lid is used so that the die may be seen inside the package.

4. Experimental results

The operation of the threshold accelerometer may be observed in Fig. 9. In Fig. 9a, the threshold accelerometer is in the open state with no applied acceleration. In Fig. 9b, an electrostatic force was applied to the proof mass, causing

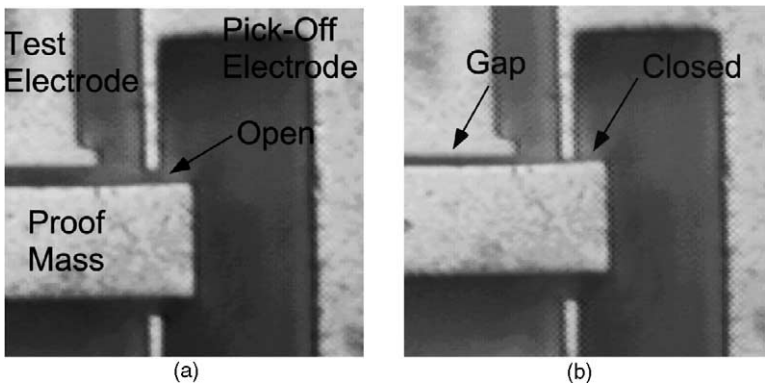

Fig. 9. Threshold accelerometer with (a) open contact and (b) closed contact.

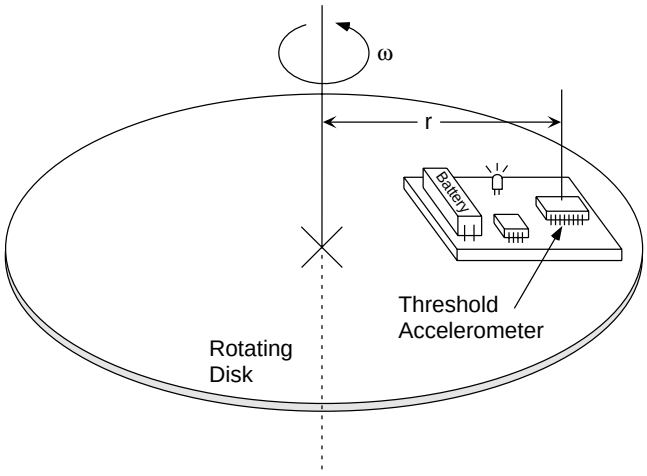

Fig. 10. Schematic of the setup used to perform the centrifuge test. The packaged threshold accelerometer array is inserted in a battery operated circuit with an LED that lights when the threshold accelerometer is triggered. The circuit is mounted on a rotating disk.

the proof mass tip to deflect as if an acceleration were applied and touch the pick-off electrode. Notice that there is still a gap between the proof mass and the test electrode.

The threshold accelerations were confirmed using a centrifuge test. Fig. 10 shows a schematic of this setup used. A packaged device was inserted in a battery operated circuit that turns on an LED when the proof mass contacts a pick-off electrode. The circuit was then attached to a horizontal rotating disk with the device under test positioned a known distance, r, from the center of the disk. A known acceleration is applied to the device under test by rotating the disk at a specific angular speed, ω. The applied acceleration is $a = \omega^2 r$. Fig. 11 shows the results from the centrifuge test. The measurements show that the actual threshold acceleration is 80% of the predicted estimate in the positive direction and 90% of the predicted estimate in the negative

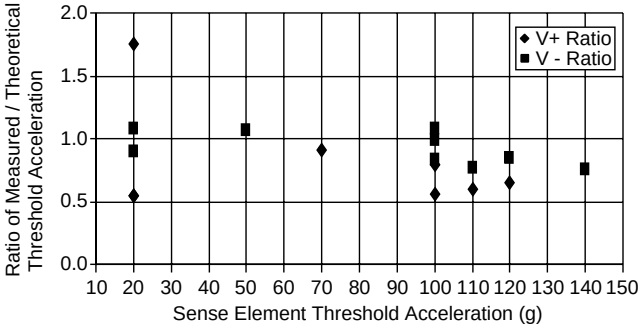

Fig. 11. Measured results obtained from the centrifuge test. The $V+$ ratio is the measured results towards the $V+$ pick-off electrode and the $V-$ ratio is the measured results towards the $V-$ pick-off electrode.

direction. There are various sources of error in this measurement, including the accuracy of the measurement of the radius from the center of the disk to the sense element under test, the measurement of the speed of the rotation, any induced forces due to any rattling or non-uniform rotation, and how level the rotating disk is. A reduction in the cantilever beam width of approximately 0.1 μm is sufficient to cause the difference between the measured and expected acceleration thresholds.

The built-in test feature of the threshold accelerometers was also used to verify the performance. Fig. 12 shows the results of the pull-in voltage test. The average pull-in voltage is 77% of the theoretical estimate. A measured pull-in voltage that is smaller than was calculated is consistent with the results obtained from the centrifuge test. Fig. 13 shows the results of the transit time test. The measurement results confirm that the threshold accelerometer can be self-tested using either the pull-in voltage test or the transit time test. The transit time test has a larger variation than the pull-in voltage test, but this is expected because the transit time test is sensitive to more parameters. The accelerometer was also tested using the capacitance sense mode. Accelerations from

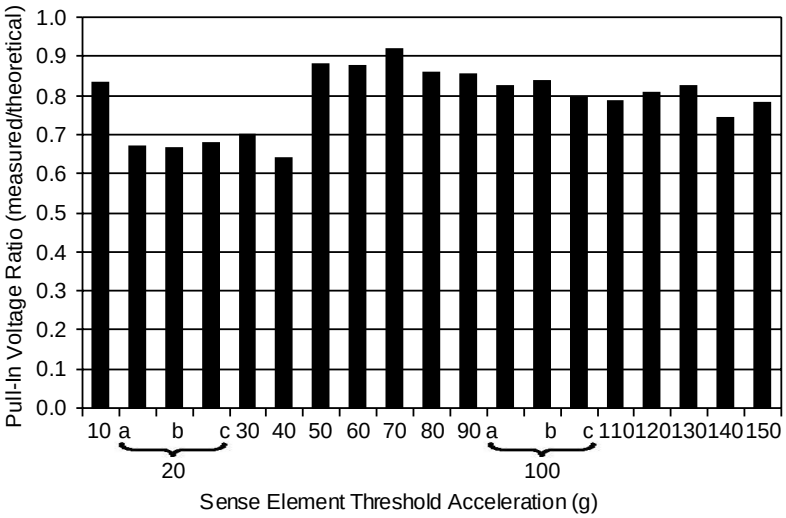

Fig. 12. Measured results from the pull-in voltage test.

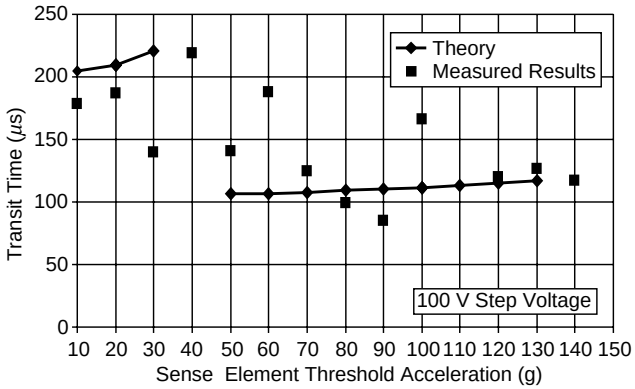

Fig. 13. Measured results from the transit time test.

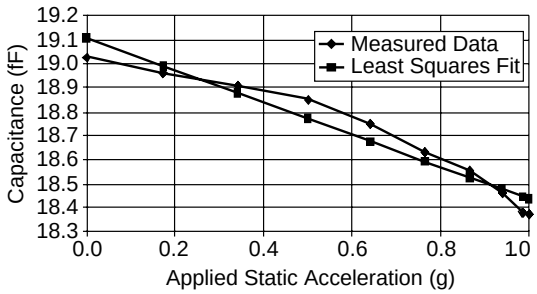

Fig. 14. Measured capacitive sense mode results for a 50 g threshold accelerometer.

0 to 1 g were applied to the accelerometer by tilting the device from 0 to 90° relative to the earth's surface. The capacitance was measured using an external capacitance meter. The results of this test using a 50 g threshold accelerometer are shown in Fig. 14. These data indicate a sensitivity of 670 aF/g, which compares well with the theoretical estimate of 780 aF/g. The graph is not a straight line because the capacitance varies non-linearly with the gap size, and the gap size varies linearly with applied acceleration.

Informally, the devices are robust. There has been no observed degradation over many months of use in hand-held demonstration circuits that have been repeatedly hit against hard surfaces and dropped. The same cannot be said of the printed circuit board holding the threshold accelerometer and demonstration circuit. The circuit board requires occasional rework. More formally, the threshold accelerometer has been electrostatically actuated and released in excess of 500,000 times with less than 1 V change in the pull-in voltage.

5. Conclusions

This effort has demonstrated a working threshold accelerometer array with very little power consumption and good sensitivity. The highest sensitivity (lowest threshold) is 10 g, considerably improved over the best reported in the past. The following improvements in reliability and robustness have helped to realize the high sensitivity devices: first, the structure is designed to minimize the strain in the cantilever spring when over-range accelerations are applied; second, the proof mass is designed so that it never contacts any electrodes that are at a high voltage during self-test; third, the use of LIGA permits very thick structures that minimize out-of-plane deformation.

The threshold accelerometer was tested with a centrifuge test, a pull-in voltage test, and a transit time test. The centrifuge test shows that the actual threshold acceleration is 80% of the designed value in the positive direction and 90% of the designed value in the negative direction. The average measured pull-in voltage is 77% of the calculated pull-in voltage. The average transit time measurements are within 10% of the theoretical values. The transit time test is a new built-in test technique that performs a more thorough test than the conventional pull-in voltage test. Finally, the devices were used in a capacitance sense mode, whereby the capacitance between the test electrode and the proof mass was measured. Measured results show a sensitivity of 670 aF/g for a 50 g threshold accelerometer, which agrees within 20% of theory.

Acknowledgements

This work was funded in part by Canopus Systems Inc., through US Army Aviation and Missile Command (AMCOM) contract DAAH01-00-C-R104. The facilities used for this research include the Wisconsin Center for Applied Microelectronics (WCAM) and the NSF supported Synchrotron Research Center (SRC) at the University of Wisconsin, Madison (Award No. DMR-0084402).

References

[1] L.M. Roylance, J.B. Angell, A batch-fabricated silicon accelerometer, IEEE Trans. Elec. Dev. ED-26 (1979) 1911–1917.
[2] P.F. Man, C.H. Mastrangelo, Surface Micromachined Shock Sensor for Impact Detection, Solid-State Sensor and Actuator Workshop, Hilton Head, 1994, pp. 156–159.
[3] Y. Loke, G.H. McKinnon, M.J. Brett, Fabrication and characterization of silicon micromachined threshold accelerometers, Sens. Actuators A 29 (1991) 235–240.
[4] C. Robinson, D. Overman, R. Warner, T. Blomquist, Problems Encountered in the Development of a Microscale g-Switch Using Three Design Approaches, in: Proceedings of the fifth International Conference on the Sensors and Actuators (Transducers '87), 1987, pp. 410–413.
[5] W.D. Frobenius, S.A. Zeitman, M.H. White, D.D. O'Sullivan, R.G. Hamel, Microminiature ganged threshold accelerometers compatible with integrated circuit technology, IEEE Trans. Electron Dev. ED-19 (1) (1972) 37–40.
[6] A. Selvakumar, N. Yazdi, K. Najafi, A wide range micromachined threshold accelerometer array and interface circuit, J. Micromech. Microeng. 11 (2) (2001) 118–125.
[7] S. McNamara, Y.B. Gianchandani, A 19-Element Shock Sensor Array For Bi-Directional Substrate-Plane Sensing Fabricated By Sacrificial LIGA, in: Proceedings of the 11th International Conference on Solid-State Sensors and Actuators (Transducers '01), Munich, Germany, June 2001, pp. 450–453.

[8] U.S. Patent No. 6,619,123.
[9] H. Guckel, High-aspect-ratio micromachining via deep X-ray lithography, Proc. IEEE 86 (8) (1998) 1586–1593.
[10] S. McNamara, A Wide Range Threshold Accelerometer Array Fabricated By A Modified LIGA Technique, Ph.D. Thesis, University of Wisconsin, Madison, 2002.
[11] J.B. Starr, Squeeze-Film Damping in Solid-State Accelerometers, IEEE Solid State Sensor and Actuator Workshop, June 1990, pp. 44–47.
[12] X. Zhang, W.C. Tang, Viscous air damping in laterally driven microresonators, in: Proceedings of the IEEE MEMS Conference, 1994, pp. 199–204.